

The angular size of dwarf stars and subgiants

Surface brightness relations calibrated by interferometry

P. Kervella^{1,2}, F. Thévenin³, E. Di Folco⁴ and D. Ségransan⁵

¹ LESIA, UMR 8109, Observatoire de Paris-Meudon, 5, place Jules Janssen, F-92195 Meudon Cedex, France

² European Southern Observatory, Alonso de Cordova 3107, Casilla 19001, Vitacura, Santiago 19, Chile

³ Observatoire de la Côte d'Azur, BP 4229, F-06304 Nice Cedex 4, France

⁴ European Southern Observatory, Karl-Schwarzschild-str. 2, D-85748 Garching, Germany

⁵ Observatoire de Genève, CH-1290 Sauverny, Switzerland

Received date / Accepted date

Abstract. The availability of a number of new interferometric measurements of Main Sequence and subgiant stars makes it possible to calibrate the surface brightness relations of these stars using exclusively direct angular diameter measurements. These empirical laws allow to predict the limb darkened angular diameters θ_{LD} of dwarfs and subgiants using their dereddened Johnson magnitudes, or their effective temperature. The smallest intrinsic dispersions of $\sigma \leq 1\%$ on θ_{LD} are obtained for the relations based on the K and L magnitudes, for instance $\log \theta_{LD} = 0.0502 (B - L) + 0.5133 - 0.2 L$ or $\log \theta_{LD} = 0.0755 (V - K) + 0.5170 - 0.2 K$. Our calibrations are valid between the spectral types A0 and M2 for dwarf stars (with a possible extension to later types when using the effective temperature), and between A0 and K0 for subgiants. Such relations are particularly useful to estimate the angular size of calibrators for long baseline interferometry from readily available broadband photometry.

Key words. Stars: fundamental parameters, Techniques: interferometric

1. Introduction

The surface brightness (hereafter SB) relations link the emerging flux per solid angle unit of a light-emitting body to its color, or effective temperature. These relations are of considerable astrophysical interest, as a well-defined relation between a particular color index and the surface brightness can provide accurate predictions of the stellar angular diameters. Such predictions are essential for the calibration of long-baseline interferometric observations. We propose in the present paper new and accurate calibrations of the SB-color relations of dwarfs and subgiants based on direct interferometric measurements of nearby members of these two luminosity classes. Our primary purpose is to establish reliable relations that can be used to predict the angular size of calibrator stars for long baseline interferometry.

After defining the surface brightness relations (Sect. 2), we discuss in Sect. 3 the sample of measurements that we selected for our calibrations (interferometric and photometric data). Sect. 4 is dedicated to the calibration of the empirical SB relations, relatively to the color indices and to the effective temperature, for stars of spectral types A0

to M2. We also derive inverse relations to estimate the effective temperature from broadband photometry and angular diameter measurements. As the established relations are intended to be used primarily to predict angular diameters, we discuss in Sect. 5 their associated error bars in this context. In Sect. 6, we search for a possible instrumental bias linked to one of the five interferometric instruments represented in our sample. Numerous versions of the SB relations have been established in the literature, mostly for giants and supergiants, and we discuss them in Sect. 7. Main Sequence stars are potentially very good calibrators for long baseline interferometry, and we discuss this particular application of our SB relations in Sect. 8.

2. Direct and inverse surface brightness relations

By definition, the bolometric surface flux $f \sim L/D^2$ is linearly proportional to T_{eff}^4 , where L is the bolometric flux of the star, D its bolometric diameter and T_{eff} its effective temperature. In consequence, $F = \log f$ is a linear function of the stellar color indices, expressed in magnitudes (logarithmic scale), and SB relations can be fitted using (for example) the following expressions:

$$F_B = a_0 (B - V)_0 + b_0 \quad (1)$$

$$F_V = a_1 (V - K)_0 + b_1 \quad (2)$$

$$F_H = a_2 (B - H)_0 + b_2 \quad (3)$$

where F_λ is the surface brightness. When considering a perfect blackbody curve, any color can in principle be used to obtain the SB. The index 0 designates the dereddened magnitudes, and the a_i and b_i coefficients represent respectively the slopes and zero points of the different versions of the SB relation. The particular expression of the SB relation $F_V(V - R)$ is also known as the Barnes-Evans (B-E) relation, and is historically the first version to have been calibrated empirically (Barnes, Evans & Pearson 1976). However, the relatively large intrinsic dispersion of the visible B-E relation has led to prefer its infrared counterparts, in particular those based on the K band magnitudes ($\lambda = 2.0 - 2.4 \mu\text{m}$), as infrared wavelengths are less affected by interstellar extinction. The surface brightness F_λ is given by the following expression (Fouqué & Gieren 1997) :

$$F_\lambda = 4.2207 - 0.1 m_{\lambda_0} - 0.5 \log \theta_{\text{LD}} \quad (4)$$

where θ_{LD} is the limb darkened angular diameter, i.e. the angular size of the stellar photosphere.

The linear expressions of the SB can be inverted easily to predict angular diameters, and give linear relations such as:

$$\log \theta_{\text{LD}} = c_1 (V - K) + d_1 - 0.2 V \quad (5)$$

for the $F_V(V - K)$ inversion. We have in this example:

$$c_1 = -2 a_1 \quad (6)$$

$$d_1 = 2 (4.2207 - b_1) \quad (7)$$

In the present paper, we will refer to both the direct and inverse relations as ‘‘SB relations’’.

3. Selected measurement sample

3.1. Angular diameters

Over the past two years, sixteen new angular diameter measurements of nearby Main Sequence and subgiant stars were obtained with the VLT Interferometer (Glindemann et al. 2000; Glindemann et al. 2003a; Glindemann et al. 2003b) equipped with the fiber-based beam combiner VINCI (Kervella et al. 2000; Kervella et al. 2003a). To complement this sample, we have searched the literature, and added to our list the measurements related to the stars of luminosity classes IV and V. Most of the visible and infrared interferometers are represented in our sample, with measurements from the NII (*Narrabri Intensity Interferometer*; Hanbury Brown, Davis & Allen 1967), the Mk III (Shao et al. 1988), the PTI (*Palomar Testbed Interferometer*; Colavita et al. 1999) and the NPOI (*Navy Prototype Optical Interferometer*; Armstrong et al. 1998). Our findings originally included

a few lunar occultation measurements, but they were rejected as they were related to variable or multiple stars, or their precision was not sufficient to give them any weight in the fitting process.

In order to obtain a consistent sample of limb darkened (LD) angular diameters, we have retained solely the uniform disk (UD) values from the literature. The conversion of these model-independent measurements to LD values was achieved using the linear LD coefficients u from Claret (2000), and the conversion formula from Hanbury Brown et al. (1974a). These coefficients are broadband, single-parameter approximations of the Kurucz (1992) model atmospheres. They are tabulated for a grid of temperatures, metallicities and surface gravities and we have chosen the closest models to the physical properties of the stars. We have considered a uniform microturbulent velocity of 2 km.s^{-1} for all stars. This single source for limb darkening corrections ensures the self-consistency of our final sample.

3.2. Photometry

All the apparent magnitudes that we have retained from the literature are expressed in the Johnson system. When available, we have preferentially kept the uncertainties given by the original authors, otherwise we applied arbitrarily a conservative error bar. The U band magnitudes were obtained from Morel et al. (1978) and Mermilliod (1986), and we adopted a ± 0.02 error. The B , V , R and I bands were obtained from several online catalogues available through VIZIER (Ochsenbein, Bauer & Marcout 2000), and we also adopted a ± 0.02 uncertainty. For the J to L infrared bands, references are not so easy to find, as many bright stars are unfortunately absent from the recent infrared surveys, like 2MASS (Cutri et al. 2003) or DENIS (Fouqué et al. 2000). We have relied on the VIZIER database to obtain the infrared magnitudes of our sample of stars. In some cases, the references we used are 30 years old, but many of them have small and reliable uncertainties. The original references of the measurements are given in the footnotes of Table 3.

3.3. Data selection

The SB relations rely on the assumption that stars behave like black bodies, i.e. that their colors are mainly governed by their effective temperature. A severe deviation from this assumption will cause a discrepancy between the actual flux per surface unit and the temperature of the star.

For instance, if there is a second, unresolved star near the main object, its additional flux will bias the spectral energy distribution. For this reason, we have rejected the binary and multiple objects for which separate photometry of the components is not available.

The presence of warm material in the circumstellar environment can also create an excess at infrared wavelengths. While this signature is most useful to identify the

stars surrounded by protoplanetary disks, it creates a bias on the measured color of the star. Some of the stars we selected are surrounded by debris disks (ϵ Eri, α PsA, τ Cet, β Leo), but the contribution of the circumstellar material is negligible, even in the infrared J to L bands. The material surrounding these stars is very cold and radiates mostly in the far infrared domain. We have rejected the measurement of β Pic from Di Folco et al. (*in prep.*), due to its large uncertainty ($\simeq 10\%$) and to the relatively high density of its edge-on circumstellar disk that could cause a significant extinction.

The fast rotating stars can deviate significantly from the black body assumption. As demonstrated by the VINCI observations of the nearby Be star α Eri (Domiciano de Souza et al. 2003), the photosphere of these objects can be deformed by their fast rotation. This creates differential limb darkening between the pole and the equator that appear to have different effective temperatures. This makes it particularly difficult to define the true photometric solid angle sustained by these objects. In addition, many fast rotating stars go through episodes of mass loss, that are likely to create a warm circumstellar environment. The presence of such hot material around the star will create a bias on the flux and color of the star. For these reasons, we have chosen to reject the known fast rotators ($v \sin i \geq 100 \text{ km.s}^{-1}$) and the Be stars from our list.

The very low mass stars *Proxima* (GJ 551, M5.5V) and *Barnard's star* (GJ 699, M4V) have been excluded from our fitting procedures for three reasons. The first one is that due to their very low effective temperatures, the molecular absorption bands dominate their spectra and lead to a significant discrepancy with the hotter stars. Second, these stars are variable, presenting occasional flares that make it difficult to estimate their magnitudes. Third, they present chromospheric activity that could bias their magnitudes in the U to V colors. However, we have kept these two stars on the SB relation figures for comparison.

The spectroscopic and eclipsing binaries are less useful for the estimation of the surface brightness relation, as it is in general impossible to measure separately the magnitudes of these stars with the required precision. For this reason, we have not included in our sample the angular diameter measurements obtained by spectroscopic or photometric methods. For the interested reader, a rather complete compilation of the measurements using these techniques can be found in the CADARS catalogue by Pasinetti-Fracassini et al. (2001).

3.4. Final sample

We report in Tables 1 and 2 the complete set of measurements that we have considered for our fit. In this table, the angular diameters θ_{UD} (uniform disk) and θ_{LD} (limb-darkened disk) are expressed in milliarcseconds (mas). The limb darkening conversion coefficient $k = \theta_{\text{LD}}/\theta_{\text{UD}}$ was computed for each star based on the ta-

bles of Claret (2000). When a physical parameter was not available in the literature, it has been estimated approximately, and appears in *italic* characters. The observation wavelength λ is given either as the name of the photometric band (V , H , K) or the actual wavelength in μm . The error bar on the angular diameter of the Sun (G2V) has been set arbitrarily to $\pm 0.1\%$. The parallaxes are from the *Hipparcos* catalogue (Perryman et al. 1997), except the α Cen value that was taken from Söderhjelm (1999), who derived it from reprocessed *Hipparcos* data. The interferometer used for each measurement is indicated in the "Instr." column.

4. Surface brightness relations

4.1. Fitting procedure

For each angular diameter measurement θ_{LD} , and based on the observed apparent magnitudes m_λ , we have computed the surface brightness F_λ in all bands, using the definition of Eq. 4. The resulting F_λ values were then fitted relatively to the colors $(C_0 - C_1)$, using a linear model. This fit was achieved using a classical χ^2 minimization taking into account the errors on both the colors and F_λ . The minimized quantity, using the slope a and zero point b as variables, is the reduced χ^2 expression:

$$\chi_{\text{red}}^2(a, b) = \frac{1}{N-2} \sum_{i=1}^N \frac{[(F_0)_i - a(C_0 - C_1)_i - b]^2}{(\sigma_{F_i})^2 + a^2(\sigma_{C_i})^2} \quad (8)$$

where we have:

- N the total number of measurements in our sample,
- $(F_0)_i$ the surface brightness of star i in band C_0 ,
- $(C_0 - C_1)_i$ the color of the star of index i computed between bands C_0 and C_1 ,
- σ_{C_i} the 1σ error bar on the chosen color of star i ,
- σ_{F_i} the 1σ error bar on the surface brightness F_0 .

The 1σ errors σ_a and σ_b are subsequently estimated from the best fit values a and b by solving numerically the expression:

$$\chi_{\text{red}}^2(a + \sigma_a, b + \sigma_b) = \chi_{\text{red}}^2(a, b) + 1. \quad (9)$$

The solutions of this equation correspond to an elliptic contour, due to the correlation between the a and b variables. It has to be projected on the a and b axis to give the error bars. The residuals $\Delta F_i = F_i - F_{\text{model}}$ are used to estimate the intrinsic dispersion $\sigma_{\text{int}}(F)$ of the surface brightness relation from:

$$\sigma_{\text{int}}^2(F) = \frac{1}{N} \sum_{i=1}^N [(\Delta F_i)^2 - (\sigma_{F_i})^2] \quad (10)$$

This process gives a total number of 72 (a, b) best fit pairs, with their associated error bars (σ_a, σ_b) , and the intrinsic dispersion σ_{int} of the data around the best fit model.

From there, we can invert these relations easily to obtain their angular diameter counterparts:

$$\log \theta_{\text{LD}} = c(C_0 - C_1) + d - 0.2 C_0 \quad (11)$$

Table 1. Angular diameters of dwarf stars (luminosity class V) measured by long-baseline interferometry (apart from the Sun). They are expressed in mas, and T_{eff} is in K. "Ref.₁" designates the reference used for T_{eff} , $\log g$ and $[\text{Fe}/\text{H}]$. When unavailable, the metallicity has been set arbitrarily to the solar value. "Ref.₂" designates the reference used for each angular diameter measurement (expressed in mas). The error bars are given in superscript close to each value.

Star	Spect.	π (mas)	Ref. ₁	T_{eff}	$\log g$	$[\text{Fe}/\text{H}]$	Instr.	Ref. ₂	λ	θ_{UD}	k	θ_{LD}
α Lyr	A0V	128.93 ^{0.55}	(a,e)	9522	3.98	-0.33	PTI	(8)	K	3.24 ^{0.01}	1.012	3.28 ^{0.01}
α Lyr	A0V	128.93 ^{0.55}	(a,e)	9522	3.98	-0.33	NII	(1)	V	3.08 ^{0.07}	1.046	3.22 ^{0.07}
α Lyr	A0V	128.93 ^{0.55}	(a,e)	9522	3.98	-0.33	Mk III	(4)	0.8	3.15 ^{0.03}	1.028	3.24 ^{0.03}
α Lyr	A0V	128.93 ^{0.55}	(a,e)	9522	3.98	-0.33	Mk III	(4)	0.55	3.00 ^{0.05}	1.046	3.13 ^{0.05}
α CMa A	A1V	379.21 ^{1.58}	(b)	9800	4.30	0.40	NII	(16)	V	5.60 ^{0.07}	1.045	5.85 ^{0.07}
α CMa A	A1V	379.21 ^{1.58}	(b)	9800	4.30	0.40	VLTI	(9)	K	5.94 ^{0.02}	1.012	6.01 ^{0.02}
α CMa A	A1V	379.21 ^{1.58}	(b)	9800	4.30	0.40	Mk III	(4)	0.8	5.82 ^{0.11}	1.027	5.98 ^{0.11}
β Leo	A3V	90.16 ^{0.89}	(g)	8570	4.26	0.20	VLTI	(10)	K	1.43 ^{0.03}	1.015	1.45 ^{0.03}
β Leo	A3V	90.16 ^{0.89}	(g)	8570	4.26	0.20	NII	(1)	V	1.25 ^{0.09}	1.052	1.31 ^{0.09}
α PsA	A3V	130.08 ^{0.92}	(g)	8760	4.22	0.43	NII	(1)	V	1.98 ^{0.13}	1.050	2.08 ^{0.14}
α PsA	A3V	130.08 ^{0.92}	(g)	8760	4.22	0.43	VLTI	(10)	K	2.20 ^{0.02}	1.014	2.23 ^{0.02}
α Cen A	G2V	747.10 ^{1.20}	(k)	5790	4.32	0.20	VLTI	(13)	K	8.31 ^{0.02}	1.024	8.51 ^{0.02}
<i>Sun</i>	G2V			5770								1919260 ^{0.1%}
τ Cet	G8V	274.18 ^{0.80}	(i)	5400	4.55	-0.40	VLTI	(10)	K	2.03 ^{0.03}	1.024	2.08 ^{0.03}
GJ 166 A	K1V	198.25 ^{0.84}	(a)	5073	4.19	-0.31	VLTI	(15)	K	1.60 ^{0.06}	1.029	1.65 ^{0.06}
α Cen B	K1V	747.10 ^{1.20}	(k)	5260	4.51	0.23	VLTI	(13)	K	5.86 ^{0.03}	1.026	6.01 ^{0.03}
ϵ Eri	K2V	310.74 ^{0.85}	(a)	5052	4.57	-0.15	VLTI	(10)	K	2.09 ^{0.03}	1.027	2.15 ^{0.03}
GJ 105 A	K3V	138.72 ^{1.04}	(a)	4718	4.50	-0.07	PTI	(12)	H, K	0.91 ^{0.07}	1.032	0.94 ^{0.07}
GJ 570 A	K4V	169.31 ^{1.67}	(a)	4533	4.79	0.02	VLTI	(15)	K	1.19 ^{0.03}	1.030	1.23 ^{0.03}
ϵ Ind A	K4.5V	275.49 ^{0.69}	(b)	4500	4.50	-0.10	VLTI	(15)	K	1.84 ^{0.02}	1.030	1.89 ^{0.02}
GJ 380	K7V	205.23 ^{0.81}	(a)	3861	4.68	-0.93	PTI	(12)	H, K	1.27 ^{0.04}	1.018	1.29 ^{0.04}
GJ 191	M1V	255.12 ^{0.86}	(b)	3524	4.87	-0.50	VLTI	(14)	K	0.68 ^{0.06}	1.016	0.69 ^{0.06}
GJ 887	M0.5V	303.89 ^{0.87}	(f)	3645	4.80	0.00	VLTI	(14)	K	1.37 ^{0.04}	1.018	1.39 ^{0.04}
GJ 205	M1.5V	175.72 ^{1.20}	(b)	3626	4.80	0.60	VLTI	(14)	K	1.12 ^{0.11}	1.020	1.15 ^{0.11}
GJ 15 A	M2V	280.26 ^{1.05}	(a)	3721	5.00	-1.40	PTI	(12)	H, K	0.98 ^{0.05}	1.017	1.00 ^{0.05}
GJ 411	M1.5V	392.52 ^{0.91}	(h)	3620	4.90	-0.20	PTI	(12)	H, K	1.41 ^{0.03}	1.019	1.44 ^{0.03}
GJ 699	M4Ve	549.30 ^{1.58}	(a)	3201	5.00	-0.90	PTI	(12)	H, K	0.99 ^{0.04}	1.018	1.00 ^{0.04}
<i>Proxima</i>	M5.5V	772.33 ^{2.42}	(f)	3006	5.19	0.00	VLTI	(14)	K	1.02 ^{0.08}	1.030	1.05 ^{0.08}

– Ref.₁ for T_{eff} , $\log g$ and $[\text{Fe}/\text{H}]$: (a) Cenarro et al. (2001); (b) Cayrel de Strobel et al. (1997); (c) Allende Prieto et al. (2002); (d) Gray et al. (2001); (e) Thévenin & Idiart (1999); (f) Ségransan et al. (2003); (g) Erspamer & North (2003); (h) Cayrel de Strobel et al. (2001); (i) Di Folco et al. (*in prep.*); (j) Morel et al. (2001); (k) Morel et al. (2000).

– Ref.₂ for angular diameters: (1) Hanbury Brown, Davis & Allen (1974b); (2) Kervella et al. (2004a); (3) Nordgren et al. (2001); (4) Mozurkewich et al. (2003); (5) Thévenin et al. (*in prep.*); (6) Boden et al. (1998); (7) Nordgren et al. (1999); (8) Ciardi et al. (2001); (9) Kervella et al. (2003b); (10) Di Folco et al. (*in prep.*); (11) Nordgren et al. (2001); (12) Lane et al. (2001); (13) Kervella et al. (2003c); (14) Ségransan et al. (2003); (15) Ségransan et al. (*in prep.*); (16) Davis et al. (1986).

The slopes and zero points are computed from the (a, b) pairs through:

$$c = -2a, \quad \sigma_c = 2\sigma_a \quad (12)$$

$$d = 2(4.2207 - b), \quad \sigma_d = 2\sigma_b \quad (13)$$

and the intrinsic dispersions $\sigma_{\text{int}}(\log \theta_{\text{LD}})$ are given by:

$$\sigma_{\text{int}}(\log \theta_{\text{LD}}) = 2\sigma_{\text{int}}(F_\lambda) \quad (14)$$

The same method was used for the fits using the effective temperature, except that no error bar was considered on the T_{eff} values from the literature (equal weighting), and we used a second degree polynomial model instead of a linear one. We minimized numerically the following χ^2_{red} expression using a, b, c as variables:

$$\chi^2_{\text{red}}(a, b, c) = \frac{1}{N-3} \sum_{i=1}^N \frac{[F_i - F_{\text{model}}(T_{\text{eff}})_i]^2}{\sigma_F^2} \quad (15)$$

where

$$F_{\text{model}}(T_{\text{eff}})_i = a (\log T_{\text{eff}})_i^2 + b (\log T_{\text{eff}})_i + c. \quad (16)$$

The error bars on each a, b and c coefficients were not computed, as the correlations existing between these coefficients make it very difficult to determine them accurately. This is justified by the fact that the astrophysical dispersion of the measurements is largely dominant over the 1σ fitting errors of the model, and the systematic errors on these coefficients can thus be considered negligible. The inversion of the resulting T_{eff} based relations is straightforward. With an expression of the form:

$$\log \theta_{\text{LD}} = d(\log T_{\text{eff}})^2 + e(\log T_{\text{eff}}) + f - 0.2C_\lambda \quad (17)$$

we have by definition:

$$d = -2a, \quad e = -2b \quad (18)$$

Table 2. Angular diameters of subgiant stars (luminosity class IV) measured by interferometry. The references and notations are given in Table 1.

Star	Spect.	π (mas)	Ref. ₁	T_{eff}	$\log g$	[Fe/H]	Instr.	Ref. ₂	λ	θ_{UD}	k	θ_{LD}
γ Gem	A0IV	31.12 ^{2.33}	(b)	9260	3.60	-0.12	NII	(1)	V	1.32 ^{0.09}	1.047	1.38 ^{0.09}
α CMi A	F5IV-V	285.93 ^{0.88}	(c)	6530	3.96	-0.05	VLTI	(2)	K	5.38 ^{0.05}	1.019	5.48 ^{0.05}
α CMi A	F5IV-V	285.93 ^{0.88}	(c)	6530	3.96	-0.05	NPOI	(11)	V	5.19 ^{0.04}	1.057	5.49 ^{0.04}
α CMi A	F5IV-V	285.93 ^{0.88}	(c)	6530	3.96	-0.05	Mk III	(4)	0.8	5.32 ^{0.08}	1.039	5.53 ^{0.08}
α CMi A	F5IV-V	285.93 ^{0.88}	(c)	6530	3.96	-0.05	Mk III	(4)	0.55	5.30 ^{0.11}	1.057	5.60 ^{0.11}
η Boo	G0IV	88.17 ^{0.75}	(a)	6003	3.62	0.25	VLTI	(5)	K	2.15 ^{0.03}	1.022	2.20 ^{0.03}
η Boo	G0IV	88.17 ^{0.75}	(a)	6003	3.62	0.25	Mk III	(4)	0.8	2.18 ^{0.02}	1.044	2.27 ^{0.03}
η Boo	G0IV	88.17 ^{0.75}	(a)	6003	3.62	0.25	Mk III	(4)	0.55	2.13 ^{0.03}	1.063	2.26 ^{0.03}
η Boo	G0IV	88.17 ^{0.75}	(a)	6003	3.62	0.25	NPOI	(11)	V	2.17 ^{0.06}	1.064	2.31 ^{0.06}
ζ Her A	G0IV	92.64 ^{0.60}	(j)	5820	3.85	0.04	Mk III	(4)	0.8	2.26 ^{0.05}	1.045	2.36 ^{0.05}
ζ Her A	G0IV	92.64 ^{0.60}	(j)	5820	3.85	0.04	Mk III	(4)	0.55	2.13 ^{0.03}	1.065	2.27 ^{0.03}
ζ Her A	G0IV	92.64 ^{0.60}	(j)	5820	3.85	0.04	NPOI	(11)	V	2.37 ^{0.08}	1.065	2.52 ^{0.09}
μ Her	G5IV	119.05 ^{0.62}	(a)	5411	3.87	0.16	Mk III	(4)	0.8	1.86 ^{0.04}	1.049	1.95 ^{0.04}
μ Her	G5IV	119.05 ^{0.62}	(a)	5411	3.87	0.16	Mk III	(4)	0.55	1.81 ^{0.03}	1.070	1.93 ^{0.03}
β Aql	G8IV	72.95 ^{0.83}	(a)	5041	3.04	-0.04	NPOI	(7)	V	2.07 ^{0.09}	1.075	2.23 ^{0.10}
η Cep	K0IV	69.73 ^{0.49}	(a)	5013	3.19	-0.19	NPOI	(7)	V	2.51 ^{0.04}	1.064	2.67 ^{0.04}
δ Eri	K0IV	110.58 ^{0.88}	(a)	4884	3.40	-0.11	VLTI	(5)	K	2.33 ^{0.03}	1.027	2.39 ^{0.03}

$$f = 2(4.2207 - c) \quad (19)$$

As in the previous case based on colors, the intrinsic dispersions $\sigma_{\text{int}}(\log \theta_{\text{LD}})$ of the angular diameter relations are given by:

$$\sigma_{\text{int}}(\log \theta_{\text{LD}}) = 2 \sigma_{\text{int}}(F) \quad (20)$$

In some cases, we could derive only upper limits of the intrinsic dispersion σ_{int} , as it was found to be smaller than the average error of the measurements (in such cases, Eq. 10 gives a negative value for σ_{int}). For these relations, such as $\log \theta_{\text{LD}}(T_{\text{eff}}, L)$, we conclude that the intrinsic dispersion is undetectable at our level of sensitivity.

4.2. Angular diameter relations based on colors

The SB relations for $UBVRIJHKL$ colors are listed in Table 4. They take the form:

$$\log \theta_{\text{LD}}(C_0, C_1) = c_\lambda(C_0 - C_1) + d_\lambda - 0.2 C_0 \quad (21)$$

where C_0 and C_1 are any two distinct colors of the Johnson system. In many cases, the dependance of the zero magnitude limb darkened angular diameter (ZMLD), defined for $C_0 = 0$, as a function of the color is not linear in reality. Thus, the linear model that we fit does not represent well the observations. In this case, we have added a note "nl" after the obtained residual dispersion. The non-linear relations should preferably not be used for predictions, though the stated dispersions include the non linearity.

In theory, there should be a perfect diagonal symmetry between the dispersions listed in Table 4. In reality, the symmetry is only approximate, due to the fact that C_0 and C_1 are not symmetric in the expression of $\log \theta_{\text{LD}}(C_0, C_1)$. Therefore, an increased dispersion of the apparent magnitudes in one band C_1 will be reflected preferentially on the $\theta_{\text{LD}}(C_0, C_1)$ dispersion, rather than on $\theta_{\text{LD}}(C_1, C_0)$. For

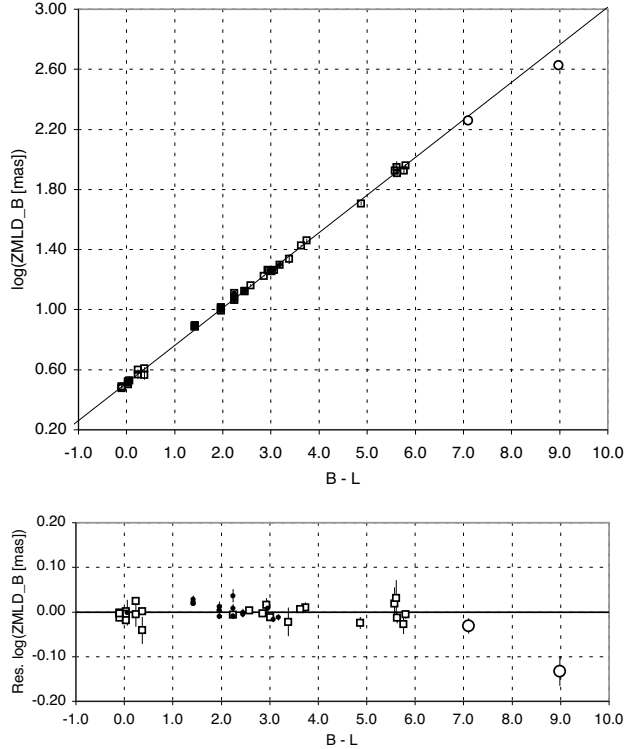


Fig. 1. Linear fit of the surface brightness relation $\log \text{ZMLD}_B(B-L)$ (upper part), and the corresponding residuals (lower part). The intrinsic dispersion of the relation is ± 0.004 on $\log \text{ZMLD}$, equivalent to a systematic error of less than 1% on the predicted angular diameters. The open circles designate GJ 699 and *Proxima*, that were excluded from the fitting procedure.

this reason, we provide both versions in Table 4, including the quasi-symmetric pairs. The best relations based

Table 3. Apparent magnitudes of the dwarf stars (upper part) and subgiants (lower part) of our sample. The uncertainty adopted on each apparent magnitude value is given in superscript.

Star	$m_U^{(a)}$	$m_B^{(b)}$	$m_V^{(b)}$	$m_R^{(c)}$	$m_I^{(c)}$	$m_J^{(d)}$	$m_H^{(d)}$	$m_K^{(d)}$	$m_L^{(d)}$
α Lyr	0.03 ^{0.02}	0.03 ^{0.02}	0.03 ^{0.02}	0.04 ^{0.02}	0.03 ^{0.02}	0.00 ^{0.02}	0.00 ^{0.01}	0.00 ^{0.01}	0.00 ^{0.01}
α CMa A	-1.51 ^{0.02}	-1.46 ^{0.02}	-1.46 ^{0.02}	-1.46 ^{0.02}	-1.45 ^{0.02}	-1.34 ^{0.03}	-1.32 ^{0.03}	-1.32 ^{0.02}	-1.36 ^{0.03}
β Leo	2.30 ^{0.02}	2.22 ^{0.02}	2.14 ^{0.02}	2.08 ^{0.02}	2.06 ^{0.02}	2.02 ^{0.01}	1.99 ^{0.09}	1.86 ^{0.09}	1.86 ^{0.09}
α PsA	1.31 ^{0.02}	1.25 ^{0.02}	1.16 ^{0.02}	1.10 ^{0.02}	1.08 ^{0.02}	1.06 ^{0.05}	1.05 ^{0.06}	0.99 ^{0.03}	1.01 ^{0.07}
α Cen A	0.92 ^{0.02}	0.70 ^{0.02}	-0.01 ^{0.02}			-1.16 ^{0.02}	-1.39 ^{0.09}	-1.50 ^{0.02}	-1.55 ^{0.09}
<i>Sun</i> ^(e)	-25.98 ^{0.02}	-26.12 ^{0.02}	-26.75 ^{0.02}	-27.12 ^{0.02}	-27.48 ^{0.02}	-27.86 ^{0.02}	-28.20 ^{0.02}	-28.22 ^{0.02}	
τ Cet	4.43 ^{0.02}	4.22 ^{0.02}	3.50 ^{0.02}	2.88 ^{0.01}	2.41 ^{0.01}	2.11 ^{0.01}	1.73 ^{0.01}	1.66 ^{0.01}	1.64 ^{0.01}
GJ 166 A	5.69 ^{0.02}	5.25 ^{0.02}	4.43 ^{0.02}	3.72 ^{0.01}	3.27 ^{0.01}	2.91 ^{0.03}	2.46 ^{0.01}	2.39 ^{0.02}	2.30 ^{0.02}
α Cen B	2.86 ^{0.02}	2.21 ^{0.02}	1.33 ^{0.02}			-0.01 ^{0.02}	-0.49 ^{0.09}	-0.60 ^{0.02}	-0.63 ^{0.09}
ϵ Eri	5.19 ^{0.02}	4.61 ^{0.02}	3.73 ^{0.02}	3.01 ^{0.02}	2.54 ^{0.02}	2.23 ^{0.03}	1.75 ^{0.03}	1.67 ^{0.01}	1.60 ^{0.05}
GJ 105 A	7.58 ^{0.02}	6.81 ^{0.02}	5.83 ^{0.02}	4.99 ^{0.02}	4.46 ^{0.02}	4.07 ^{0.03}	3.52 ^{0.03}	3.45 ^{0.03}	3.43 ^{0.03}
GJ 570 A	7.88 ^{0.02}	6.82 ^{0.02}	5.71 ^{0.02}	4.72 ^{0.02}	4.18 ^{0.02}	3.82 ^{0.02}	3.27 ^{0.02}	3.15 ^{0.02}	3.11 ^{0.02}
ϵ Ind A	6.74 ^{0.02}	5.75 ^{0.02}	4.69 ^{0.02}	3.81 ^{0.02}	3.25 ^{0.02}	2.83 ^{0.02}	2.30 ^{0.02}	2.18 ^{0.02}	2.12 ^{0.02}
GJ 380	9.23 ^{0.02}	7.94 ^{0.02}	6.59 ^{0.02}	5.36 ^{0.02}	4.56 ^{0.02}	3.98 ^{0.03}	3.32 ^{0.03}	3.19 ^{0.03}	3.11 ^{0.03}
GJ 191	11.64 ^{0.02}	10.40 ^{0.02}	8.86 ^{0.02}			5.77 ^{0.02}	5.27 ^{0.02}	5.05 ^{0.02}	4.86 ^{0.02}
GJ 887	9.99 ^{0.02}	8.83 ^{0.02}	7.35 ^{0.02}			4.20 ^{0.02}	3.60 ^{0.02}	3.36 ^{0.02}	3.20 ^{0.02}
GJ 205	10.63 ^{0.02}	9.44 ^{0.02}	7.97 ^{0.02}	6.53 ^{0.02}	5.39 ^{0.02}	4.77 ^{0.02}	4.06 ^{0.02}	3.86 ^{0.02}	3.83 ^{0.02}
GJ 15 A	10.88 ^{0.02}	9.63 ^{0.02}	8.07 ^{0.02}	6.72 ^{0.02}	5.53 ^{0.02}	4.86 ^{0.03}	4.25 ^{0.03}	4.02 ^{0.02}	3.87 ^{0.03}
GJ 411	10.13 ^{0.02}	9.00 ^{0.02}	7.49 ^{0.02}	5.98 ^{0.02}	4.76 ^{0.02}	4.13 ^{0.03}	3.56 ^{0.03}	3.35 ^{0.03}	3.20 ^{0.03}
GJ 699	12.57 ^{0.02}	11.28 ^{0.02}	9.54 ^{0.02}	7.71 ^{0.02}	6.10 ^{0.02}	5.30 ^{0.02}	4.77 ^{0.02}	4.52 ^{0.02}	4.18 ^{0.02}
<i>Proxima</i>	14.56 ^{0.02}	13.02 ^{0.02}	11.05 ^{0.02}	8.68 ^{0.02}	6.42 ^{0.02}	5.33 ^{0.02}	4.73 ^{0.02}	4.36 ^{0.03}	4.04 ^{0.02}
γ Gem	1.97 ^{0.02}	1.92 ^{0.02}	1.92 ^{0.02}	1.86 ^{0.02}	1.87 ^{0.02}	1.87 ^{0.02}	1.83 ^{0.02}	1.85 ^{0.03}	1.87 ^{0.09}
α CMi A	0.82 ^{0.02}	0.79 ^{0.02}	0.37 ^{0.02}	-0.05 ^{0.02}	-0.28 ^{0.02}	-0.40 ^{0.03}	-0.60 ^{0.03}	-0.65 ^{0.03}	-0.68 ^{0.03}
η Boo	3.46 ^{0.02}	3.26 ^{0.02}	2.68 ^{0.02}	2.24 ^{0.02}	1.95 ^{0.02}	1.67 ^{0.02}	1.39 ^{0.01}	1.35 ^{0.01}	1.30 ^{0.02}
ζ Her A	3.67 ^{0.02}	3.46 ^{0.02}	2.81 ^{0.02}	2.30 ^{0.02}	1.98 ^{0.02}	1.77 ^{0.01}	1.42 ^{0.01}	1.38 ^{0.01}	1.30 ^{0.06}
μ Her	4.57 ^{0.02}	4.17 ^{0.02}	3.42 ^{0.02}	2.89 ^{0.02}	2.51 ^{0.02}	2.13 ^{0.01}	1.80 ^{0.01}	1.74 ^{0.01}	1.72 ^{0.02}
β Aql	5.07 ^{0.02}	4.58 ^{0.02}	3.72 ^{0.02}	3.06 ^{0.02}	2.57 ^{0.02}	2.19 ^{0.02}	1.70 ^{0.01}	1.65 ^{0.02}	1.61 ^{0.02}
η Cep	4.96 ^{0.02}	4.35 ^{0.02}	3.43 ^{0.02}	2.76 ^{0.02}	2.27 ^{0.02}	1.80 ^{0.05}		1.22 ^{0.02}	1.17 ^{0.09}
δ Eri	5.13 ^{0.02}	4.46 ^{0.02}	3.54 ^{0.02}	2.82 ^{0.02}	2.32 ^{0.02}	1.95 ^{0.01}	1.49 ^{0.02}	1.40 ^{0.01}	1.36 ^{0.02}

– References:

(a) Morel et al. (1978), Mermilliod (1986).

(b) Morel et al. (1978), Hoffleit & Warren (1991), Perryman et al. (1997).

(c) Morel et al. (1978), Bessell et al. (1998), Ducati et al. (2002).

(d) Glass (1974), Glass (1975), Mould & Hyland (1976), Morel et al. (1978), Leggett (1992), Ducati et al. (2002), Kidger & Martín-Luis (2003), the 2MASS catalogue (Cutri et al. 2003).

(e) We referred to Colina et al. (1996) for the apparent magnitudes of the Sun.

on the K band (showing residual dispersions below 1% on the angular diameter θ_{LD}) are the following:

$$\log \theta_{LD} = 0.0535 (B - K) + 0.5159 - 0.2 K \quad (22)$$

$$\log \theta_{LD} = 0.0755 (V - K) + 0.5170 - 0.2 K. \quad (23)$$

and the best relations for the L band are:

$$\log \theta_{LD} = 0.0412 (U - L) + 0.5167 - 0.2 L \quad (24)$$

$$\log \theta_{LD} = 0.0502 (B - L) + 0.5133 - 0.2 L \quad (25)$$

$$\log \theta_{LD} = 0.0701 (V - L) + 0.5139 - 0.2 L \quad (26)$$

$$\log \theta_{LD} = 0.1075 (R - L) + 0.5128 - 0.2 L. \quad (27)$$

These expressions are valid at least over the range of colors defined by our sample (Tables 1 and 2). In terms of

spectral types, the angular diameter predictions can be considered reliable between A0 and M2 for dwarfs, and between A0 and K0 for subgiants. There are indications (Fig. 1) that the infrared relations are valid down to the spectral type M4V of GJ 699, but show some discrepancy for the M5.5V star *Proxima*. The established relations are likely to be valid also for subgiants of spectral types later than KOIV, but this cannot be verified based on our sample. It should be stressed that they are applicable only to single stars, and the presence of a non resolved stellar companion contributing for a significant fraction of the measured flux will bias the predicted angular diameters. As more than half of the Main Sequence stars are binary or multiple stars, care should be taken in the application of these relations.

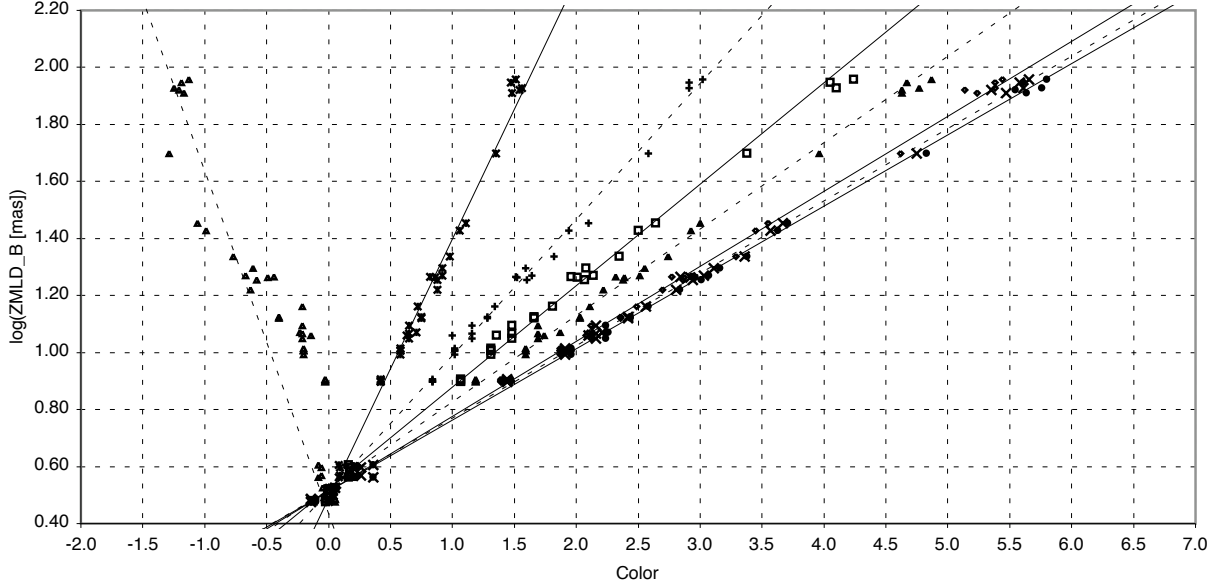


Fig. 2. Johnson B band $ZMLD_B$ relations as a function of colors. The error bars have been omitted for clarity, and the fitted models are represented alternatively as solid and dashed lines. From left to right, using the colors: $(B-U)$, $(B-V)$, $(B-R)$, $(B-I)$, $(B-J)$, $(B-H)$, $(B-K)$, $(B-L)$. A clear non linearity is visible on the $(B-U)$ based relation.

4.3. Angular diameter relations based on effective temperatures

Table 5 gives the best fit model coefficients for the relations $\theta_{LD}(T_{\text{eff}}, C_\lambda)$, defined as:

$$\log \theta_{LD} = d(\log T_{\text{eff}})^2 + e(\log T_{\text{eff}}) + f - 0.2 C_\lambda \quad (28)$$

The smallest residuals are obtained for the relations based on T_{eff} and the K or L magnitudes, with an upper limit on the 1σ dispersion of 1.0% (the true dispersion is undetectable from our data):

$$\log \theta_{LD} = 0.8470 x^2 - 7.0790 x + 15.2731 - 0.2 K$$

$$\log \theta_{LD} = 0.6662 x^2 - 5.6609 x + 12.4902 - 0.2 L$$

where $x = \log T_{\text{eff}}$. The range of validity of the T_{eff} based relations is 3600–10000 K for dwarfs, and 4900–9500 K for subgiants. As shown on Fig. 3, there are indications that the infrared relations are valid for dwarfs with T_{eff} down to ~ 3000 K.

4.4. $T_{\text{eff}}(\theta_{LD}, m_\lambda)$ relations

By inverting the relations established in Sect. 4.3, it is possible to predict the effective temperature of the observed stars based on their angular diameter and broadband magnitude in a single band. As in the previous sections, we assume a zero interstellar extinction, and the relations are valid only for dereddened magnitudes. The formulation of the $T_{\text{eff}}(\theta_{LD}, m_\lambda)$ laws is easily derived analytically. From Eq. 28, we obtain the $\log T_{\text{eff}}$ through the expression:

$$\log T_{\text{eff}} = \frac{-\sqrt{4d \log \theta_{LD} + 0.8d C_\lambda + e^2 - 4df} - e}{2d} \quad (29)$$

Table 5. SB relations using the magnitude C_λ and the effective temperature T_{eff} of the star to obtain the limb darkened angular diameter θ_{LD} (in mas): $\log \theta_{LD}(T_{\text{eff}}, C_\lambda) = d(\log T_{\text{eff}})^2 + e \log T_{\text{eff}} + f - 0.2 C_\lambda$. The 1σ residual dispersions are given in percents of the LD angular diameter.

C_λ	σ	d	e	f
U	5.93%	5.6391	-46.4505	96.0513
B	6.33%	3.6753	-30.9671	65.5421
V	5.90%	3.0415	-25.4696	53.7010
R	4.76%	2.1394	-18.0221	38.3497
I	2.28%	0.9847	-8.7985	19.9281
J	1.19%	0.9598	-8.3451	18.5204
H	1.38%	1.1684	-9.6156	20.2779
K	$\leq 1.00\%$	0.8470	-7.0790	15.2731
L	$\leq 1.00\%$	0.6662	-5.6609	12.4902

that can be rewritten as

$$\log T_{\text{eff}} = -\sqrt{g \log \theta_{LD} + h C_\lambda + i + j} \quad (30)$$

where

$$g = \frac{1}{d}, \quad h = \frac{0.2}{d}, \quad (31)$$

$$i = \frac{e^2}{4d^2} - \frac{f}{d}, \quad j = \frac{-e}{2d}. \quad (32)$$

The intrinsic dispersion of the $\log T_{\text{eff}}$ relations can be approximated from the intrinsic dispersion of the $\log \theta_{LD}$ relations, as we have $\sigma_{\text{int}}(\log \theta_{LD}) \ll 1$:

$$\sigma_{\text{int}}(\log T_{\text{eff}}) = 0.5 \sqrt{g} \sigma_{\text{int}}(\log \theta_{LD}) \quad (33)$$

Table 4. Surface brightness relations using *UBVRIJHKL* based colors to obtain the limb darkened angular diameter θ_{LD} (in mas) as a function of the magnitude and color of the star through: $\log \theta_{LD}(C_0, C_1) = c_\lambda(C_0 - C_1) + d_\lambda - 0.2 C_0$. The residual dispersions are given in percents of the LD angular diameter. The 1σ error bars on each coefficient are given in superscript, *multiplied by 1000* to reduce the length of each line, i.e. $0.5822^{3.2}$ stands for 0.5822 ± 0.0032 . When the data departs significantly from our linear fit and presents a detectable non linearity, the dispersion is mentioned in *italic* characters, and we have added the note "nl". The dispersions smaller than 5% are mentioned in bold characters: they mark the relations that are the most suitable to predict stellar angular sizes.

$C_0 \downarrow$	$C_1 \rightarrow U$	B	V	R	I	J	H	K	L
c_U		1.2701 ^{11.8}	0.5822 ^{3.2}	0.3925 ^{1.7}	0.3178 ^{1.1}	0.2805 ^{1.0}	0.2509 ^{0.8}	0.2437 ^{0.8}	0.2407 ^{0.8}
d_U		0.6607 ^{7.9}	0.5532 ^{4.5}	0.5393 ^{3.5}	0.5384 ^{3.1}	0.5351 ^{3.0}	0.5206 ^{2.9}	0.5217 ^{2.7}	0.5184 ^{2.9}
σ_U		57.8% <i>nl</i>	17.9% <i>nl</i>	10.6% <i>nl</i>	7.88% <i>nl</i>	5.05% <i>nl</i>	3.06%	2.76%	1.92%
c_B	-1.0923 ^{10.4}		0.9095 ^{6.9}	0.4771 ^{2.2}	0.3557 ^{1.4}	0.3029 ^{1.0}	0.2630 ^{0.8}	0.2538 ^{0.7}	0.2501 ^{0.9}
d_B	0.6542 ^{7.0}		0.4889 ^{1.1}	0.5116 ^{0.1}	0.5235 ^{0.1}	0.5242 ^{0.1}	0.5134 ^{1.0}	0.5158 ^{0.1}	0.5133 ^{0.1}
σ_B	59.2% <i>nl</i>		9.17% <i>nl</i>	4.75% <i>nl</i>	4.98% <i>nl</i>	3.07%	1.89%	$\leq 1.00\%$	$\leq 1.00\%$
c_V	-0.3846 ^{2.3}	-0.7083 ^{7.4}		0.7900 ^{8.4}	0.4550 ^{2.9}	0.3547 ^{2.0}	0.2893 ^{1.6}	0.2753 ^{1.4}	0.2694 ^{1.4}
d_V	0.5513 ^{3.4}	0.4889 ^{5.7}		0.5217 ^{6.4}	0.5332 ^{4.0}	0.5310 ^{3.6}	0.5148 ^{3.2}	0.5175 ^{2.9}	0.5146 ^{3.1}
σ_V	18.0% <i>nl</i>	9.18% <i>nl</i>		8.53% <i>nl</i>	8.30% <i>nl</i>	4.75%	1.85%	1.01%	$\leq 1.00\%$
c_R	-0.1966 ^{1.0}	-0.2792 ^{1.7}	-0.5842 ^{5.1}		0.7404 ^{6.4}	0.4647 ^{3.2}	0.3405 ^{2.5}	0.3158 ^{1.9}	0.3041 ^{1.8}
d_R	0.5351 ^{2.4}	0.5109 ^{3.0}	0.5251 ^{4.7}		0.5570 ^{5.2}	0.5392 ^{4.0}	0.5119 ^{3.8}	0.5158 ^{3.1}	0.5144 ^{3.3}
σ_R	11.1% <i>nl</i>	5.02% <i>nl</i>	8.63% <i>nl</i>		14.5% <i>nl</i>	8.43% <i>nl</i>	2.88%	2.05%	2.52%
c_I	-0.1210 ^{0.7}	-0.1587 ^{1.1}	-0.2609 ^{2.0}	-0.5998 ^{7.6}		0.9079 ^{19.8}	0.4318 ^{6.0}	0.3833 ^{4.5}	0.3707 ^{4.6}
d_I	0.5351 ^{1.9}	0.5207 ^{2.3}	0.5296 ^{2.8}	0.5416 ^{4.7}		0.5233 ^{7.6}	0.5089 ^{4.4}	0.5140 ^{3.7}	0.5097 ^{4.0}
σ_I	8.30% <i>nl</i>	5.34% <i>nl</i>	8.73% <i>nl</i>	12.1% <i>nl</i>		10.8% <i>nl</i>	5.83% <i>nl</i>	3.84%	3.30%
c_J	-0.0818 ^{0.6}	-0.1043 ^{0.9}	-0.1581 ^{1.4}	-0.2842 ^{3.2}	-0.7198 ^{16.9}		0.6280 ^{16.0}	0.5214 ^{10.6}	0.4840 ^{9.4}
d_J	0.5325 ^{1.9}	0.5216 ^{2.2}	0.5276 ^{2.4}	0.5299 ^{3.2}	0.5197 ^{6.5}		0.4990 ^{5.8}	0.5066 ^{4.9}	0.5078 ^{4.8}
σ_J	5.13% <i>nl</i>	3.12%	4.98%	7.26% <i>nl</i>	10.9% <i>nl</i>		10.44% <i>nl</i>	5.86% <i>nl</i>	4.08%
c_H	-0.0513 ^{0.5}	-0.0625 ^{0.6}	-0.0892 ^{0.9}	-0.1376 ^{1.8}	-0.2290 ^{4.0}	-0.4312 ^{12.1}		1.8747 ^{58.8}	1.1714 ^{27.7}
d_H	0.5189 ^{1.6}	0.5138 ^{1.8}	0.5145 ^{1.9}	0.5138 ^{2.3}	0.5093 ^{2.9}	0.5013 ^{4.4}		0.5352 ^{7.5}	0.5271 ^{6.2}
σ_H	2.67%	1.24%	1.12%	2.06%	5.53% <i>nl</i>	10.31% <i>nl</i>		17.2% <i>nl</i>	13.0% <i>nl</i>
c_K	-0.0440 ^{0.4}	-0.0535 ^{0.6}	-0.0755 ^{0.8}	-0.1144 ^{1.4}	-0.1805 ^{2.8}	-0.3192 ^{7.4}	-1.7040 ^{55.1}		3.0857 ^{33.9}
d_K	0.5202 ^{1.6}	0.5159 ^{1.6}	0.5170 ^{1.7}	0.5168 ^{1.9}	0.5149 ^{2.3}	0.5089 ^{3.4}	0.5336 ^{7.0}		0.6258 ^{3.6}
σ_K	2.58%	$\leq 1.00\%$	$\leq 1.00\%$	1.60%	3.67%	5.87% <i>nl</i>	17.6% <i>nl</i>		26.9% <i>nl</i>
c_L	-0.0412 ^{0.5}	-0.0502 ^{0.6}	-0.0701 ^{0.8}	-0.1075 ^{1.4}	-0.1696 ^{2.9}	-0.2826 ^{6.4}	-0.9843 ^{24.1}	-2.8950 ^{115.7}	
d_L	0.5167 ^{1.7}	0.5133 ^{1.8}	0.5139 ^{1.9}	0.5128 ^{2.1}	0.5101 ^{2.5}	0.5081 ^{3.3}	0.5245 ^{5.4}	0.5309 ^{12.4}	
σ_L	$\leq 1.00\%$	$\leq 1.00\%$	$\leq 1.00\%$	$\leq 1.00\%$	2.43%	3.61%	13.1% <i>nl</i>	26.3% <i>nl</i>	

The corresponding coefficients and dispersions are given in Table 6. The K band relation presents the smallest intrinsic dispersion ($\sigma \leq 0.60\%$), corresponding to a systematic uncertainty of less than 40 K on the predicted temperature of a G2V star:

$$\log T_{\text{eff}} = 4.1788 - \sqrt{1.1806 \log \theta_{LD} + 0.2361 K - 0.5695}$$

However, we would like to stress that the uncertainty on the measured apparent magnitudes can easily be dominant, as a ± 0.03 error on K will translate into a $\pm 1.7\%$ error on T_{eff} , nearly three times larger than the intrinsic dispersion.

Considering that photometry at an absolute level of ± 0.01 is not available for all stars, the T_{eff} predictions from different bands can be averaged, taking carefully into account the statistical and systematic errors of each relation used, in order to reach the intrinsic dispersion level. In addition, such an averaging process should not be done for

stars affected by interstellar or circumstellar extinction, as it will affect differently each photometric band.

4.5. Metallicity

A possible source of natural dispersion of the SB relations is the presence of deep absorption lines in the spectrum of the stars. This effect is stronger for stars that have a high metal content. However, as shown on Fig. 5, no correlation could be evidenced between the residuals of the least dispersed relation $\theta_{LD}(L, B - L)$ and the metallicity $[\text{Fe}/\text{H}]$. This is an indication that our SB relations are valid at least for metallicities between -0.5 and $+0.5$ dex, and probably also for lower values. The two metal-deficient stars of Fig. 5 are GJ 15 A ($[\text{Fe}/\text{H}] = -1.40$ dex) and GJ 699 ($[\text{Fe}/\text{H}] = -0.90$ dex, not included in our fits). For typical stars of the solar neighborhood, our relations are thus always applicable.

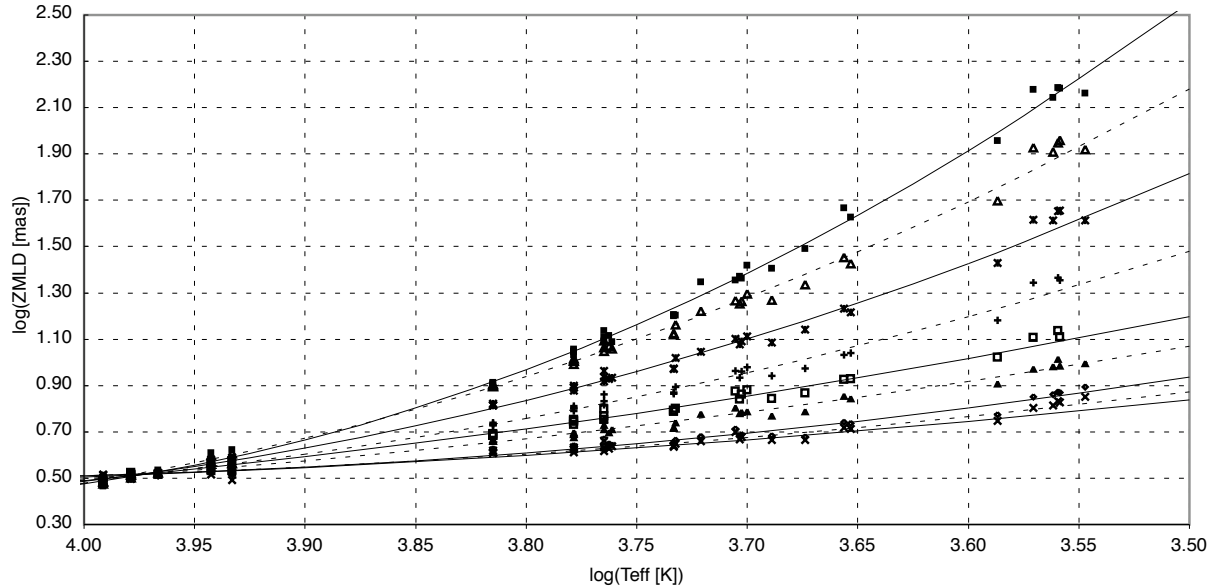


Fig. 4. $ZMLD_\lambda$ relations as a function of the effective temperature. The error bars have been omitted for clarity, and the fitted models are represented alternatively as solid and dashed lines. From top to bottom, using the zero magnitude reference colors U , B , V , R , I , J , H , K and L .

Table 6. $T_{\text{eff}}(\theta_{\text{LD}}, m_\lambda)$ relations to obtain the effective temperature: $\log T_{\text{eff}} = -\sqrt{g} \log \theta_{\text{LD}} + h C_\lambda + i + j$. The 1σ residual dispersions are given in percents of the effective temperature T_{eff} (expressed in K).

C_λ	σ	g	h	i	j
U	1.19%	0.1773	0.0355	-0.0703	4.1186
B	1.57%	0.2721	0.0544	-0.0850	4.2128
V	1.61%	0.3288	0.0658	-0.1249	4.1870
R	1.57%	0.4674	0.0935	-0.1848	4.2120
I	1.13%	1.0155	0.2031	-0.2788	4.4675
J	0.60%	1.0419	0.2084	-0.3975	4.3472
H	0.63%	0.8559	0.1712	-0.4230	4.1149
K	$\leq 0.60\%$	1.1806	0.2361	-0.5695	4.1788
L	$\leq 0.60\%$	1.5010	0.3002	-0.6977	4.2486

5. Sources of uncertainty on the predicted diameters

Several observational and astrophysical sources of uncertainty add up to create the total error bar on the predicted angular diameters:

- *intrinsic dispersion of the empirical relation:* as discussed above, the best relations have intrinsic dispersions below 1%. It should be stressed that their predictions cannot be averaged to reduce this systematic uncertainty. However, the predictions from independent colors (such as $V-K$ and $B-L$) can be averaged to reduce the statistical uncertainty on the predictions due to the error bars on the photometric measurements. In this process, the systematic uncertainties of each relation *cannot* be reduced and have to be carefully taken

into account. This is essential as the calibrations have been obtained for all colors from the same sample of stars, and the resulting systematic errors are therefore highly correlated.

- *uncertainties on the apparent magnitudes:* combining the high precision magnitudes available in the visible with the infrared magnitudes produced by the 2MASS and DENIS surveys should enable to retrieve the visible-infrared color indices with a precision better than ± 0.02 mag. However, we would like to stress that the uncertainty on the apparent magnitude measurements can easily be the largest contributor to the predicted angular diameter error bars. The true error bars on the photometric measurements have to be estimated accurately in order to obtain reasonable uncertainties on the predicted angular sizes.
- *interstellar extinction and circumstellar matter:* for the sample of nearby stars that was considered for our fits, the interstellar extinction is negligible: apart from γ Gem at 32 pc, all stars are located closer than 15 pc. However, our SB relations are strictly valid only for extinction corrected magnitudes. The uncertainty on the assumed color excess $E(B-V)$ (for instance) will translate into an additional uncertainty on the dereddened magnitudes. The presence of a significant amount of circumstellar matter around the star will also affect its spectral properties, and can be difficult to detect.

6. Comparison between interferometers

The residuals of the fits of the least dispersed relations (based on infrared colors) allow us to examine if system-

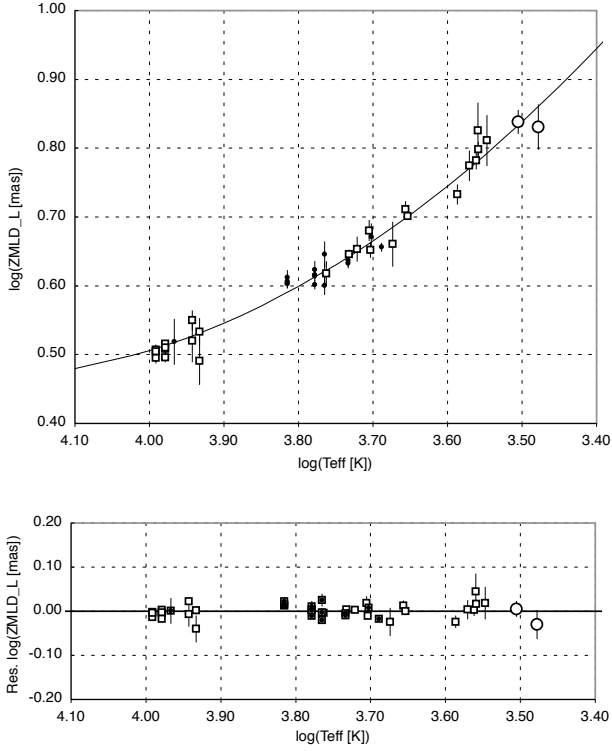


Fig. 3. Second degree polynomial fit of $ZMLD_L(\log T_{\text{eff}})$ (upper part) and the corresponding residuals (lower part). The coefficients are given in Table 5, and correspond to a relation of the form $\log ZMLD_L = d(\log T_{\text{eff}})^2 + e(\log T_{\text{eff}}) + f$. The open circles designate GJ 699 and *Proxima*, that were excluded from the fit (see Sect. 3.3), though they are consistent with the model within their error bars.

atic discrepancies are detectable between the five interferometers represented in our sample. For each instrument, we have computed the average residuals of its pertaining measurements, and the 1σ error bar resulting from the averaging of their respective errors. The results are presented in Table 7.

We observe that the average residuals are below 1.5% in terms of ZMLD for all instruments. In addition, all the deviations are below 1σ , and can therefore be fully explained by random statistical dispersion. As a remark, the agreement between the VLTI/VINCI results and the Mk III is remarkable, with no systematic deviation detectable at a level a few tenths of a percent. This is especially encouraging as these two instruments are observing at very different wavelengths (visible and K band, respectively).

This comparison exercise relies implicitly on the assumption that the considered $ZMLD_0(C_0 - C_1)$ relations are applicable to each instrument’s subsample of stars, down to the precision of each individual measurement. This may not be the case for all stars, but the agreement that we observe is a worst case, and the true agreement is in any case very satisfactory.

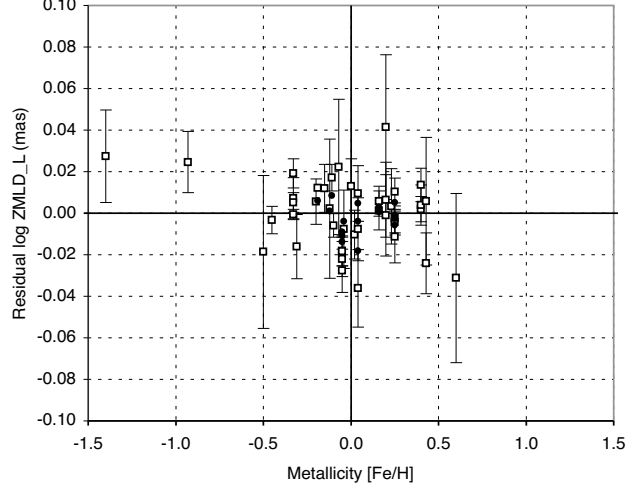


Fig. 5. Residuals of the fit of $ZMLD_L(L, B-L)$ as a function of the metallicity $[Fe/H]$ of the star. Dwarfs are represented by open squares, and subgiants by solid dots. No correlation is visible among the stars of our sample.

7. Previous calibrations and other luminosity classes

Previous calibrations of the SB relations for dwarfs have been derived by Di Benedetto (1998) and Van Belle (1999a). These two authors relied on the limited sample of hot dwarfs observed with the Narrabri intensity interferometer (Hanbury Brown et al. 1974a; Hanbury Brown et al. 1974b). The agreement of our calibration with the work by Van Belle (1999a) is satisfactory within 1σ for the $(V, V-K)$ relation, but there is a difference of about 2σ on the slope of the $(B, B-K)$ relation. As the fit obtained by this author is based on a small range of colors, we attribute this moderate discrepancy to an underestimation of the true error bar on the slope, even on the restricted quoted range of validity $(-0.6 \leq B-K \leq +2.0)$.

Several calibrations of the SB relations for giants have been proposed in the recent years, thanks to the availability of a number of direct interferometric measurements of this class of stars. Van Belle (1999a) has used a sample of 190 giants, complemented by 67 carbon stars and Miras measured with the PTI (Van Belle et al. 1999b), IOTA (e.g. Dyck et al. 1998) and lunar occultation observations (e.g. Ridgway et al. 1982) to calibrate the $F_V(V-K)$ relation of giant and supergiant stars. Welch (1994) and Fouqué & Gieren (1997) proposed a calibration of the SB relations of Cepheids based on an extrapolation of the corresponding relations of giants. Among the supergiants, Cepheids occupy a particular place. The observations of these variable stars by interferometry, intended primarily to study their pulsation, have resulted in the measurement of several of these objects (Mourard et al. 1997; Lane et al. 2000; Nordgren et al. 2000; Kervella et al. 2001; Lane et al. 2002; Kervella et al. 2004b). Based on these observations, Nordgren et al. (2002) have established dedicated SB relations for Cepheids, and they find a satisfactory

Table 7. Comparison between interferometers. The average residuals of the fits of $ZMLD_B$ and $ZMLD_V$ for the K and L based colors are given together with the corresponding 1σ error bars. All values are expressed in percents of the $ZMLD$ values. All the residuals are compatible with zero within their 1σ error bars.

Instrument	N	$\Delta ZMLD_B(B-K)$	$\Delta ZMLD_V(V-K)$	$\Delta ZMLD_B(B-L)$	$\Delta ZMLD_V(V-L)$
PTI	5	$+0.48 \pm 0.89\%$	$+0.82 \pm 0.94\%$	$+0.63 \pm 0.89\%$	$+0.89 \pm 0.93$
NII	5	$+1.02 \pm 1.42\%$	$+1.03 \pm 1.46\%$	$+1.03 \pm 1.58\%$	$+1.02 \pm 1.63$
Mk III	11	$-0.11 \pm 0.56\%$	$-0.12 \pm 0.57\%$	$-0.06 \pm 0.64\%$	-0.11 ± 0.66
NPOI	5	$-1.20 \pm 1.20\%$	$-1.23 \pm 1.24\%$	$-1.23 \pm 1.24\%$	-1.39 ± 1.53
VLTI/VINCI	16	$-0.05 \pm 0.49\%$	$-0.07 \pm 0.51\%$	$-0.07 \pm 0.51\%$	-0.11 ± 0.68

agreement with previous works. From these studies, it appears that the SB relations found for giants and supergiants are similar to the ones determined in the present paper for dwarfs and subgiants, especially their visible-infrared versions. This means qualitatively that any two stars of class I-V with similar magnitudes in two bands will present approximately the same angular diameters.

8. Main Sequence stars as calibrators for long-baseline interferometry

8.1. The need for small and nearby calibrators

Interferometric observations are generally based on interspersed observations of a scientific target and a calibrator. The angular size of the calibrator is supposed to be known *a priori*, and the observed fringe contrast is used to estimate the instrumental transfer function (also called system visibility). The catalogue of calibrators assembled by Cohen et al. (1999), and customized to interferometry by Bordé et al. (2002), consists mainly of K giants with angular diameters of about 2 mas. While this size is well adapted to short baseline observations (up to a few tens of meters in the infrared), these stars are too large angularly to serve as calibrators for the hectometric baselines of the VLTI, the CHARA array (McAlister et al. 2000) or the NPOI (Armstrong et al. 1998). In addition, it is foreseen to implement on the VLTI shorter wavelengths than the K band currently accessible with VINCI. For instance, the AMBER instrument (Petrov et al. 2000) will allow observations in the J band. The two fold increase in angular resolution will naturally require significantly smaller calibrators than the Cohen et al. (1999) catalogue.

A fundamental problem with distant stars is that the reddening corrections are uncertain. This means that it is highly desirable to use nearby stars as calibrators, located within a few tens of parsecs. In this respect, giant stars are not well suited due to their large linear dimensions, but dwarfs and subgiants are ideally adapted to provide small and well-defined calibrators.

Another advantage of Main Sequence stars is that their strong surface gravity results in a compact atmosphere and a well-defined photosphere. Their disk appears sharper than the giants, for which the precise definition of the limb darkened disk angular diameter at a level of less than 1% can be difficult, in particular for the later spectral types. As an example, a discussion about the M4III

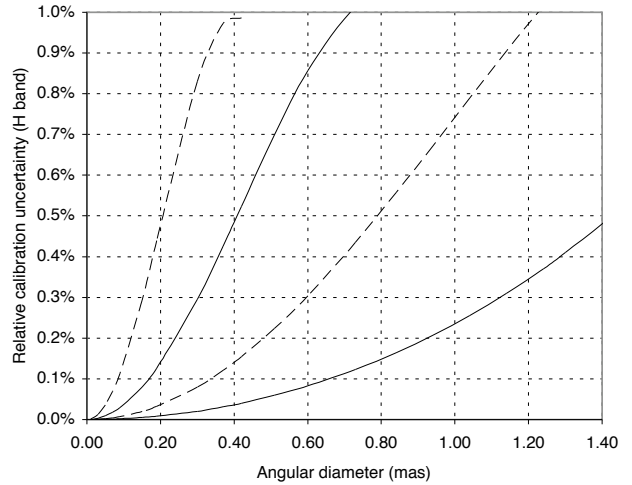


Fig. 6. Precision achievable on the measurement of the interferometric efficiency as a function of the angular diameter of the calibrator, predicted using the $(B, B-L)$ SB relation ($\leq 1.0\%$ dispersion). From left to right, the curves refer to baselines of 800, 400, 200 and 100 m, in the H band.

giant ψ Phe can be found in Wittkowski, Aufdenberg & Kervella (2004).

8.2. Calibration precision vs. brightness

It is possible to estimate the maximum angular size of calibrator stars in order to obtain a given relative precision on the calibration of the interferometric efficiency. Fig. 6 shows the achievable precision on the interferometric efficiency using the $(B, B-L)$ relation determined in Sect. 4.2 ($\sigma \leq 1.0\%$), as a function of the angular diameter of the calibrator star, for four different baselines (100, 200, 400 and 800 m), in the H band. These baselines are representative of the existing or foreseen interferometers (Keck, PTI, VLTI, CHARA, NPOI and OHANA, sorted by increasing maximum baseline). The horizontal scale of Fig. 6 can be adapted for other wavelengths or other baselines by scaling it linearly while maintaining constant the B/λ ratio.

If we now set a limit of 0.5% on the acceptable systematic uncertainty on the interferometric efficiency, we can compute the apparent magnitude of the Main Sequence

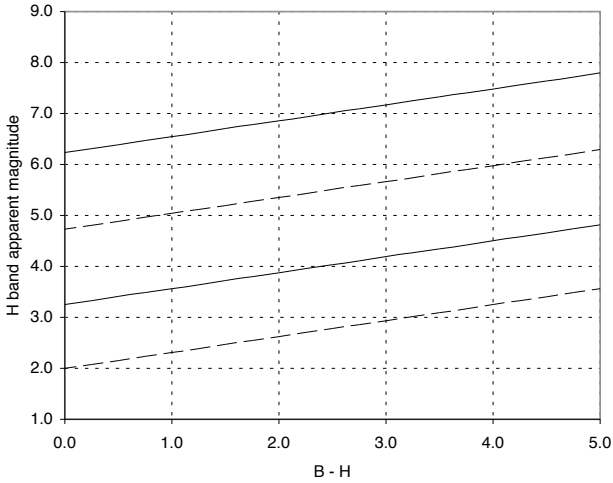


Fig. 7. Apparent magnitude in the H band of the calibrators suitable to obtain a relative precision of 0.5% on the calibration of the interferometric efficiency, as a function of the $B - H$ color. From top to bottom, the curves refer to baselines of 800, 400, 200 and 100 m, in the H band.

calibrators that should be used as a function of their color. The result is presented on Fig. 7 as a function of the $B - H$ color, for different baseline lengths and interferometric observations in the H band. From this figure, it can be concluded that suitable calibrators for extremely long baseline observations will have to be faint. Let us consider the example of the OHANA interferometer (original idea proposed by Mariotti et al. 1996), whose longest foreseen baseline is 800 m. The H band magnitude of the calibrators necessary to obtain a relative systematic visibility error of 0.5% will be between $m_H = 6$ and 8, depending on the spectral type. This is rather faint, even for large aperture light collectors, but is feasible with OHANA.

As an alternative, it is possible to build (through time consuming observations) a secondary network of brighter and larger calibrators based on the small angular diameter ones, but there will always be a limitation attached to the fact that calibrators have to be observed in the first lobe of their visibility function. For OHANA, this sets a hard limit of $\simeq 0.5$ mas to the calibrator angular size, and even ≤ 0.4 mas to obtain a visibility of at least 0.3. This corresponds to apparent magnitudes of $m_H = 5$ to 7 in the H band, one magnitude brighter than the primary network.

For the longest baseline of the VLTI (200 m), calibrator magnitudes between $m_H = 3$ and 5 will be sufficient, clearly in the accessible domain of the AMBER beam combiner (Petrov et al. 2000) with the 1.8 m Auxiliary Telescopes (Koehler et al. 2002). The creation of a secondary network of calibrators should therefore not be necessary.

It should be stressed that the present conclusions regarding magnitudes are not limited to dwarf stars, as giants and supergiants follow comparable surface brightness

Table 8. Photometry (upper part) and predicted limb darkened angular diameters θ_{LD} (lower part) of the planet-hosting stars 51 Peg A and HD 209458 A.

	51 Peg A	HD 209458 A
m_V	5.50 ± 0.01	7.65 ± 0.01
m_K	3.97 ± 0.01	6.31 ± 0.03
$\theta_{LD}(K, V - K)$	0.689 ± 0.011 mas	0.228 ± 0.004 mas

relations. This means that the magnitude ranges defined above will be almost the same for other luminosity classes. A decisive advantage of dwarfs is that for the same apparent magnitude, they will be much closer than the more luminous classes, and therefore significantly less affected by interstellar extinction.

8.3. Example of diameter prediction

As a practical application, we have chosen the two stars 51 Peg A (HD 217014) and HD 209458 A. The former hosts the first planet discovered around a solar type star (Mayor & Queloz 1995), and the latter presents planetary transits (Charbonneau et al. 2000). We selected these two stars because they were observed extensively using different techniques and did not show any large amplitude photometric variability. They therefore represent good examples of stable, well known stars, and are ideal candidates for the prediction of their angular size using the SB relations determined in the present paper.

Table 8 presents the predicted angular diameters of the two stars for the $(V, V - K)$ version of the SB relation. The m_V magnitudes are from *Hipparcos* (Perryman et al. 1997) for both stars, with an arbitrary error bar of ± 0.01 , while the K band infrared magnitudes were taken from Ducati et al. (2002) for 51 Peg A, and from the 2MASS catalogue (Cutri et al. 2003) for HD 209458 A.

For 51 Peg A, we obtain a predicted angular diameter of $\theta_{LD} = 0.689 \pm 0.011$ mas. The corresponding value for HD 209458 A is $\theta_{LD} = 0.228 \pm 0.004$ mas. These angular sizes can be translated into linear radii using the *Hipparcos* parallaxes (Perryman et al. 1997), $\pi_{51 \text{ Peg A}} = 65.10 \pm 0.76$ mas and $\pi_{\text{HD 209458 A}} = 21.24 \pm 1.00$ mas. We obtain $R_{51 \text{ Peg A}} = 1.138 \pm 0.023 R_{\odot}$ and $R_{\text{HD 209458 A}} = 1.154 \pm 0.059 R_{\odot}$. HD 209458 A is a particularly interesting object, as Brown et al. (2001) have been able to estimate directly its linear radius through the deconvolution of the light curve of the transit. They obtain a value of $R_{\text{HD 209458 A}} = 1.146 \pm 0.050 R_{\odot}$, in remarkable agreement with our $(K, V - K)$ prediction. The bulk of the $\pm 5\%$ uncertainty comes from the error on the *Hipparcos* parallax, the relative error on the angular size being only $\pm 2\%$.

The direct measurement of the angular diameter of 51 Peg A is within the capabilities of the existing very long baseline interferometers (several hundred meters), but this is not true for HD 209458 A. Its 0.228 mas size would require baselines of more than 800 m to be resolved at visible wavelengths (several kilometers in the infrared). Such

baselines are not presently available or scheduled. And even so, the calibration of these observations would be extremely difficult, as the calibrator would have to be very faint. More generally, carefully calibrated surface brightness relations are currently the only method to estimate precisely ($\pm 1\%$) the angular size of solar type stars fainter than $m_V = 7$.

9. Conclusion

The laws that we established between the angular size and broadband colors (or effective temperature) are strictly empirical. Our best relations present a very small intrinsic dispersion, down to less than 1%. They can be used to predict the angular sizes of A0–M2 dwarfs and A0–K0 subgiants from simple, readily available broadband photometry. On one hand, Gray et al. (2003) have recently published an extensive survey of the spectral properties of nearby stars within 40 pc, including estimates of their effective temperatures. On the other hand, several large catalogues (2MASS, DENIS,...) provide high precision magnitudes of these stars in the infrared. From the cross-comparison of these sources, the SB relations determined in the present paper make it possible to assemble a catalogue of calibrators for interferometry that will practically not be affected by interstellar extinction, multiplicity or circumstellar material biases. These resulting angular diameter predictions will provide a reliable basis for the calibration of long baseline interferometric observations.

Acknowledgements. P.K. acknowledges support from the European Southern Observatory through a post-doctoral fellowship. This research has made an extensive use of the SIMBAD and VIZIER online databases at CDS, Strasbourg (France).

References

- Allende Prieto, C., Asplund, M., Garcia Lòpez, R. J., & Lambert, D. L. 2002, *ApJ*, 567, 544
- Armstrong, J. T., Mozurkewich, D., Rickard, L. J., et al. 1998, *ApJ*, 496, 550
- Barnes, T. G., Evans, D. S., & Parson, S. B. 1976, *MNRAS*, 174, 503
- Bessell, M. S., Castelli, F., & Plez, B. 1998, *A&A*, 333, 231
- Boden, A. F., Van Belle, G. T., Colavita, M. M. 1998, *ApJ*, 504, 39
- Bordé, P., Coudé du Foresto, V., Chagnon, G., & Perrin, G. 2002, *A&A*, 393, 183
- Brown, T. M., Charbonneau, D., Gilliland, R. L., Noyes, R. W., Burrows, A. 2001, *ApJ*, 552, 699
- Cayrel de Strobel, G., Soubiran, C., Friel, E.D., Ralite, N., & Francois, P., 1997, *A&AS*, 124, 299
- Cayrel de Strobel G., Soubiran C., & Ralite N. 2001, *A&A*, 373, 159
- Cenarro, A. J., Cardiel, N., Gorgas, J., et al. 2001, *MNRAS*, 326, 959
- Charbonneau, D., Brown, T. M., Latham, D. W., & Mayor, M. 2000, *ApJ*, 522, L145
- Ciardi, D. R., Van Belle, G. T., Akeson, R. L., et al. 2001, *ApJ*, 559, 1147
- Claret, A. 2000, *A&A*, 363, 1081
- Cohen, M., Walker, R. G., Carter, B., et al. 1999, *AJ*, 117, 1864
- Colavita, M. M., Wallace, J. K., Hines, B. E., et al. 1999, *ApJ*, 510, 505
- Colina, L., Bohlin, R. C., & Castelli, F. 1996, *AJ*, 112, 307
- Cutri, R. M., Skrutskie, M. F., Van Dyk, S., et al. 2003, Univ. of Massachusetts and IPAC, <http://www.ipac.caltech.edu/2mass>.
- Davis, J., & Tango, W. J. 1986, *Nature*, 323, 234
- Di Benedetto, G. P. 1998, *A&A*, 339, 858
- Di Folco, E., Thévenin, F., Kervella, P., et al. 2004, *in prep.*
- Domiciano de Souza, A., Kervella, P., Jankov, S., et al. 2003, *A&A*, 407, L47
- Ducati, J. R. 2002, NASA Ref. Pub. 1294
- Dyck, H. M., Van Belle, G. T., & Thompson, R. R. 1998, *AJ*, 116, 981
- Erspamer, D., & North, P. 2003, *A&A* 398, 1121
- Fouqué, P., & Gieren, W. P. 1997, *A&A*, 320, 799
- Fouqué P., Chevallier, L., Cohen, M., et al. 2000, *A&AS*, 141, 313
- Glass, I. S. 1974, *Month. Not. of Astron. Soc. South Africa*, 33, 53
- Glass, I. S. 1975, *MNRAS* 171, 19
- Glindemann, A., Abuter, R., Carbognani, F., et al. 2000, *Proc. SPIE*, 4006, 2
- Glindemann, A., Argomedo, J., Amestica, R., et al. 2003a, *Proc. SPIE*, 4838, 89
- Glindemann, A., Argomedo, J., Amestica, R., et al. 2003b, *ApSS*, 286, 1
- Gray, R. O., Graham, P. W., & Hoyt, S. R. 2001, *AJ*, 121, 2159
- Gray, R. O., Corbally, C. J., Garrison, R. F., Mc Fadden, M. T. & Robinson, P. E. 2003, *AJ*, 126, 2048
- Hanbury Brown, R., Davis, J., Allen, L. R. 1967, *MNRAS*, 137, 375
- Hanbury Brown, R., Davis, J., Lake, J. W., & Thompson, R. J. 1974a, *MNRAS*, 167, 475
- Hanbury Brown, R., Davis, J., & Allen, L. R. 1974b, *MNRAS*, 167, 121
- Hoffleit, D., & Warren W. H. 1991, *The Bright Star Catalogue*, 5th Revised Ed., Astronomical Data Center, NSSDC/ADC
- Kervella, P., Coudé du Foresto, V., Glindemann, A., Hofmann, R. 2000, *Proc. SPIE*, 4006, 31
- Kervella, P., Coudé du Foresto, V., Perrin, G., et al. 2001, *A&A*, 367, 876
- Kervella, P., Gilton, Ph., Ségransan, D., et al. 2003a, *Proc. SPIE*, 4838, 858
- Kervella, P., Thévenin F., Morel P., Bordé, P., & Di Folco, E. 2003b, *A&A*, 408, 681
- Kervella, P., Thévenin, F., Ségransan, D., et al. 2003c, *A&A*, 404, 1087
- Kervella, P., Thévenin F., Morel P., et al. 2004a, *A&A*, 413, 251
- Kervella, P., Nardetto, N., Bersier, D., Mourard, D., & Coudé du Foresto V. 2004b, *A&A*, in press, astro-ph/0311525
- Kidger, M. R., & Martín-Luis, F. 2003, *AJ*, 125, 3311
- Koehler, B., Flebus, C., Dierickx, P., et al. 2002, *ESO Messenger*, 110, 21
- Kurucz, R. L. 1992, *IAU Symp. 149: The Stellar Populations of Galaxies*, 149, 225
- Lane, B. F., Kuchner, M. J., Boden, A. F., Creech-Eakman, M., & Kulkarni S. R. 2000, *Nature*, 407, 485
- Lane, B. F., Boden, A. F., & Kulkarni, S. R., 2001, *ApJ*, 551, L81

- Lane, B. F., Creech-Eakman, M., & Nordgren, T. E. 2002, *ApJ*, 573, 330
- Leggett, S. K. 1992, *ApJS*, 82, 35
- Mariotti, J.-M., Coudé du Foresto, V., Perrin, G., Peiqian Zhao, & Léna, P., 1996, *A&AS*, 116, 381
- McAlister, H. A., Bagnuolo, W. G., ten Brummelaar, T. A., et al. 2000, *Proc. SPIE*, 4006, 465
- Mayor, M., & Queloz, D. 1995, *Nature*, 378, 355
- Mermilliod J.-C. 1986, Catalogue of Eggen's UBV data (unpublished, available through SIMBAD)
- Morel, M., & Magnenat, P. 1978, *A&AS*, 34, 477
- Morel, P., Provost, J., Lebreton, Y., Thévenin, F., & Berthomieu, G. 2000, *A&A*, 363, 675
- Morel, P., Berthomieu, G., Provost, J., & Thévenin, F. 2001, *A&A*, 379, 245
- Mould, J. R., & Hyland A. R. 1976, *ApJ*, 208, 399
- Mourard, D., Bonneau, D., Koechlin, L., et al. 1997, *A&A*, 317, 789
- Mozurkewich, D., Armstrong, J. T., Hindsley, R. B., et al. 2003, *AJ*, 126, 2502
- Nordgren, T. E., Germain, M. E., Benson, J. A., et al. 1999, *AJ*, 118, 3032
- Nordgren, T. E., Armstrong, J. T., Germain, M. E., et al. 2000, *ApJ*, 543, 972
- Nordgren, T. E., Sudol, J. J., & Mozurkewich, D. 2001, *AJ*, 122, 2707
- Nordgren, T. E., Lane, B. F., Hindsley, R. B., & Kervella, P. 2002, *AJ*, 123, 3380
- Ochsenbein, F., Bauer, P., Marcout, J. 2000, *A&AS*, 143, 221
- Pasinetti-Fracassini, L. E., Pastori, L., Covino, S., & Pozzi, A. 2001, *A&A*, 367, 521
- Petrov, R., Malbet, F., Richichi, A., et al. 2000, *Proc. SPIE*, 4006, 68
- Perryman, M. A. C., Lindegren, L., Kovalevsky, J., et al., *The Hipparcos Catalogue*, 1997, *A&A*, 323, 49
- Ridgway, S. T., Jacoby, G. H., Joyce, R. R., & Wells, D. C., 1982, *AJ*, 87, 1044
- Shao, M., Colavita, M. M., Hines, B. E., et al. 1988, *ApJ*, 327, 905
- Ségransan, D., Kervella, P., Forveille, T., Queloz, D. 2003, *A&A*, 397, L5
- Ségransan, D., Kervella, P., Forveille, T., Queloz, D. 2004, *in prep.*
- Söderhjelm, S. 1999, *A&A* 341, 121
- Thévenin F., & Idiart, T. P. 1999, *ApJ*, 521, 753
- Thévenin, F., Kervella, P., et al., 2004, *in prep*
- Van Belle, G. T. 1999a, *PASP*, 11, 1515
- Van Belle, G. T., Lane, B. F., Thompson, R. R., et al. 1999b, *AJ*, 117, 521
- Welch, D. L. 1994, *AJ*, 108, 1421
- Wittkowski, M., Aufdenberg, J. P., & Kervella, P. 2004, *A&A*, 413, 711